Investigating Summer 2022 Arctic Cyclone Structure and Evolution

Ariel Jacobs

A thesis submitted in partial fulfillment of the
requirements for the degree of

Master of Science

University of Washington

2024

Committee:

Cecilia Bitz, Chair

Edward Blanchard-Wrigglesworth

Robert Wood

Alexandria Anderson-Frey

Program Authorized to Offer Degree:
Atmospheric Sciences

University of Washington

Abstract

Investigating Summer 2022 Arctic Cyclone Structure and Evolution

Ariel Jacobs

Chair of the Supervisory Committee:
Prof. Cecilia Bitz
Atmospheric Sciences

Arctic cyclones have large impacts on sea-ice redistribution and are hazardous to communities in the region, yet the structure and evolution of summer Arctic cyclones is not fully understood. The structure and evolution of summer 2022 Arctic cyclones are investigated using Community Earth Systems Model (CESM) atmosphere-only simulations nudged to European Centre for Medium Range Weather Forecasts (ECMWF) fifth generation reanalysis (ERA5). We explore the bias of cyclones compared to ERA5 simulated in CESM when nudging to the full-atmosphere, above the boundary layer only, and above the troposphere only. Full-atmosphere and above the boundary layer only nudged runs compare reasonably well to ERA5 in cyclone location, structure, and evolution. A case study analysis demonstrated a warm core cyclone interacted with a tropospheric polar vortex (TPV) before maturation, which showcased the transition between a vertically and horizontally asymmetric storm to a more axisymmetric storm at maturation in both CESM and ERA5. A composite analysis of Arctic cyclones in the full-atmosphere and above the boundary layer only nudged runs showed warm core and cold core cyclones had distinct thermodynamic and dynamic structures, but combining all cyclones leads to similar structure as in previous studies. The biases compared to ERA5 when nudging CESM only above the boundary layer

or above the troposphere are largely due to the different boundary layer and cloud physics parameterizations in ERA5 and CESM, so observational comparison is warranted to contextualize these results. Future work includes observational comparison, utilizing a higher resolution grid, and evaluating the boundary layer parameterization in CESM.

TABLE OF CONTENTS

LIST OF FIGURES

LIST OF TABLES

ACKNOWLEDGMENTS

I would like to thank my advisor Prof. Cecilia Bitz for all of her support and guidance throughout this project. I would like to thank Prof. Edward Blanchard-Wrigglesworth for his insightful contributions to our discussions regarding the model experiments and importance of tropospheric polar vorticies. I would like to thank Prof. Robert Wood for serving on my committee and being a true student advocate. I would like to thank Prof. Alexandria Anderson-Frey for her synoptic expertise and for serving on my committee. I would like to thank my close friends and family for their love and support during these last couple of years especially my best friend Aaron, my partner Kyle, and my cat Prince. Finally, I would like to thank the Office of Naval Research for funding support through the National Defense Science and Engineering Graduate (NDSEG) fellowship.

Chapter 1
INTRODUCTION

In recent decades, Arctic sea-ice extent has been rapidly decreasing, and under a high emissions scenario, the Arctic could be seasonally ice free by 2050 [1]. Sea-ice loss affects the global radiation budget by lowering the polar albedo allowing more radiation to be absorbed. This feedback, known as the ice-albedo feedback, contributes to Arctic amplification, or the warming of the Arctic faster than the global mean. Sea ice loss endangers the fragile Arctic ecosystem and the indigenous communities who rely on sea ice for travel, food, and cultural practices [2, 3]. Sea ice loss also impacts shipping and transportation routes increasing the need for search and rescue missions. Summer Arctic cyclones have large impacts on sea-ice redistribution and are among the most challenging cyclones to forecast on Earth. High winds associated with summer Arctic cyclones can increase ice drift speed, leading to increased deformation and increased ice-albedo feedback [4]. Heat and moisture transport from summer Arctic cyclones can increase cloudiness and thus exposure to longwave radiation leading to sea-ice melt [5]. As sea-ice continues to melt and thin, cyclones cause more ice drift and upwelling of warm water furthering sea-ice loss [6]. These impacts are particularly amplified by extreme cyclones [7] such as the great Arctic cyclone of 2012 [8] and the January 2022 Arctic cyclone [9]. However, sea-ice loss is dependent on the location relative to the Arctic cyclone. Sea-ice actually increases to the west of the Arctic cyclone and decreases to the east of the Arctic cyclone in a cardinal

North framework. [10]. These changes in sea ice are driven by the cyclonic rotation of the Arctic cyclone and the existing North-South gradient of sea ice concentration and thickness. In addition, the surface flux anomalies affect the melt rate in summer. There is more absorption of net radiation to the east of the storm and less absorption to the west of the storm [10].

Many questions remain about mechanisms that control Arctic cyclones' formation, spatial scale, and long lifetimes. Most studies have focused on the importance of the upper troposphere, including tropospheric polar vortices, on the formation and evolution of Arctic cyclones. Cyclonic tropospheric polar vortices or TPVs are anomalously cold vortices at the tropopause with radii under 1500 km that generate positive potential vorticity anomalies. They form from stratospheric intrusions of anomalously warm, dry air into anomalously cold, moist tropospheric air due to diabatic heating in the form of absorption of longwave radiation. [11]. TPVs have long lifetimes of up to a couple months long and are attributed to cyclogenesis and cyclone longevity [12, 13, 14]. Around half of all Arctic cyclones are associated with TPVs [15] including extreme cyclones such as the great summer 2012 Arctic cyclone [16] and the summer 2016 Arctic cyclone [13, 17].

More recently, the role of the atmospheric boundary layer in summer Arctic cyclogenesis and evolution has been explored. The Arctic atmospheric boundary layer (ABL) is weakly convective over sea ice [18], and low level baroclinic zones are mostly confined to regions near coastlines. The main region of low-level baroclinicity is the Arctic Frontal Zone between the coast of Eurasia and the Arctic Ocean [19, 20]. During the summer, the ocean near the coastline is ice-free creating a large temperature gradien between the land and open ocean. This thermodynamically driven baroclinicity at the surface helps to intensify summer Arctic cyclones.

While the literature has described such surface-based sources of baroclinicity and the association with TPVs, the structure and evolution of summer Arctic cyclones is still an open question. The first theoretical model of a summer Arctic cyclone, based on two case studies, showcased an axisymmetric storm with a warm stratosphere and cold troposphere resembling a larger TPV [17]. However, a composite of many Arctic cyclones showed they are horizontally heterogeneous with a warm, moist eastern sector and a cool, dry western sector with respect to the cyclone center [10]. In addition, analysis using a potential vorticity approach found there can be lower-level dominated cyclones as well as upper-troposphere dominated cyclones at the maximum growth rate [21, 22]. The lower-level dominant cyclones are influenced by the ABL, are driven by frictional generation of potential vorticity, and are typically warm core and baroclinic systems. The upper-level dominant cyclones are typically associated with TPVs and are cold-core and barotropic storms. The evolution of Arctic Cyclones has also begun to be explored. A study using a storm centered and storm rotated approach of 100 intense cyclones found the thermodynamic structure of summer Arctic cyclones transitions from an asymmetric cyclone with distinct warm and cold sectors before minimum sea level pressure to axisymmetric cold core storms after maturation [23] as presented in [17]. They hypothesize that summer Arctic cyclones do not fully undergo occlusion leading to an axisymmetric storm and longer lifetimes. More recently, a study of over 9300 cyclones determined the structure of Arctic cyclones during estimated cyclogenesis and cyclolysis to be asymmetric [24] similar to [10].

Global climate models have also been used to analyze Arctic cyclones. Under historical forcing, global climate models are generally able to reproduce the location and track density of Arctic cyclones but struggle to reproduce short-lived cyclones and summer cyclones originating in the Arctic [25]. Under future projection scenarios, summer Arctic cyclone activity is expected to increase in part due to the strengthening of the Arctic frontal zone [20, 26]. However, these types of studies do not allow for case study analyses that can be compared to observations.

Our aim is to investigate the structure and evolution of Arctic cyclones during May - September 2022 using atmosphere-only global climate model simulations nudged to reanalysis at varying vertical thresholds. By constraining the model by different amounts in each run, we are able to see model biases that are associated with the boundary layer scheme and free-running in the troposphere. This will inform analyses in future studies. In addition, atmosphere-only runs provide a baseline for comparing the effects of sea ice in eventual fully-coupled runs.

In this study we aim to address the following questions:

1. Where and by how much must a model be constrained to produce a realistic Arctic surface cyclone?

2. How does the structure of an Arctic cyclone change from maximum growth rate to minimum sea level pressure?

3. Is warm core versus cold core a valid dichotomy?

In the next section (section 2), we describe the datasets including the reanalysis used and the model runs and the methods including nudging and the cyclone tracking algorithm. In section 3.1 we describe the model statistical comparison with reanalysis. We examine an Arctic cyclone case study in section 3.2 and composites in section 3.3. We discuss our findings in section 4 and conclude and suggest avenues for future work in section 5.

Chapter 2
DATA AND METHODS

2.1 Reanalysis Data

We used European Centre for Medium Range Weather Forecasts (ECMWF) fifth generation reanalysis (ERA5) data [27] for model evaluation during the entire May 2022- September 2022 study period. ERA5 data was regrided the model 1° resolution for comparison. Cyclone tracking, a cyclone-centered analysis of case studies, and cyclone compositing are employed.

2.2 Model Simulations

We used the Community Earth Systems Model (CESM) version 2.2 [28] with the ARCTIC [29] and Finite Volume (FV) [30] grids in atmosphere-only mode (sea ice extent and sea surface temperatures were specified). The ARCTIC grid is built on the spectral-element (SE) dynamical core, which utilizes a cubed sphere domain with refined resolution in the Arctic. The finest resolution in the Arctic is about 27.8 km, while the rest of the globe is 1°, or about 100 km. The FV grid is built on the finite volume (FV) dynamical core, which utilizes a standard latitude longitude grid and 1° resolution throughout the globe. We completed one experiment on the ARCTIC grid and five on the finite volume grid. Setting up the ARCTIC grid with nudging and our preliminary examination of its output was a major activity of this master's project, but the results will not be featured in this Thesis because the root mean squared differences between CESM runs on ARCTIC and FV grids were small and ERA5 root mean squared errors (RMSEs) were similar in magnitude. Hence, the FV grid proved to be sufficient for the objectives defined in the Introduction. In addition, the FV runs were much less computationally expensive. We plan to explore the ARCTIC run in more detail in the future.

We used historical forcing through 2022 that was an extension of the inputs used for CESM in CMIP6 [28] provided by Adam Herrington (personal communication). We use historical forcing instead of a climate projection used in previous studies (eg. [31]) to better characterize the climate state during our study period. The temperature and horizontal winds were nudged to atmospheric reanalysis (ERA5) to permit a case study analysis. Additionally, nudging in CESM has shown to better represent the polar climate compared to relying on historical forcing in a large ensemble [31]. Nudging is performed by relaxing the model variables toward the target reanalysis data using the following equation:

$$
\begin{aligned}
&\frac{dx}{dt} = F(x) + F_{nudge}, \\
&F_{nudge} = \alpha[O(t'_{next}) - x(t)]/\tau,
\end{aligned}
\tag{2.1}
$$

where α and τ are parameters that control the location and timescale of the nudging, respectively. In our case, α was set to one inside our nudging window and set to zero outside the nudging window. We used a nudging window of 30° N-90° N to constrain the midlatitudes as well since more than half of all Arctic cyclones originate in the midlatitudes [32].

The parameters used in each model experiment are in Table 2.1. The nudging level refers to the lowest vertical level that is nudged out of 32 possible levels, where levels are numbered starting at the top of the model. Frequency refers to the frequency of the ERA5 data used. The nudging type describes whether the nudging target data ($O(t'_{next})$) is interpolated linearly to the model time step or instead the target is fixed for the frequency interval and then steps abruptly. For every experiment, the zonal wind, meridional wind, and temperature were nudged.

We ran experiment with a three-hourly target frequency to gauge if increased target frequency was warranted, and decided the RMSE values were similar and small enough in the 6 hourly run to keep the nudging frequency at 6 hours. The experiments in bold will be the focus of the thesis. The model employs hybrid sigma levels. One experiments nudges all vertical-levels, referred to as the full-atmosphere (FA) run. Another nudges upward from the 25th vertical level (on average above 850 hPa), referred to as the above the boundary layer (ABL) run. The final experiment nudges upward from 17th vertical level run (above 300 hPa), referred to as the above the troposphere (AT) run. By constraining the model by different amounts in each run, we are able to see model biases that are associated with the boundary layer scheme and the free-running troposphere. The current boundary layer scheme implemented in CESM2.2 is the Cloud Layers Unified By Binormals (CLUBB) scheme, which is a unified planetary boundary layer scheme that uses a double Gaussian assumed PDF in conjunction with a higher-order closure method to parameterize turbulence, shallow convection, and cloud macrophysics [33, 34]. This will inform analyses in future studies.

Grid	Variables	Frequency	Time period	Nudging level/Type
ARCTIC SE	U,V,T	6-hourly	May-Sept 2022	All/next-step
FV	U,V,T	6-hourly	May-Sept 2022	All/next-step
FV	U,V,T	3-hourly	May 2022	All/next-step
FV	**U,V,T**	**6-hourly**	**May-Sept 2022**	**All/linear**
FV	**U,V,T**	**6-hourly**	**May-Sept 2022**	**25/linear**
FV	**U,V,T**	**6-hourly**	**May-Sept 2022**	**17/linear**

Table 2.1: Model Run Parameters

2.3 Arctic Cyclone Tracking Algorithm

An Arctic Cyclone tracking algorithm was developed to track the location and minimum sea level pressure of Arctic cyclones during the May 2022-September 2022 study period. The algorithm defines the Arctic as $> 65°$ N, but the algorithm starts tracking storms at 60° N to account for midlatitude cyclone propagation. Geopotential heights greater than 1500 m are masked from the search. The algorithm works by searching for the minimum sea level pressure and finding the grid points within 1200 km of that value. If the spatially averaged sea level pressure gradient of those grid points is greater than 7.5 hPa per 1000 km and there are no masked values in the selected grid points, a cyclone is identified. The specified pressure gradient follows the method outlined in [35]. If the identified cyclone is within 600 km of an existing cyclone from the previous time step (an hour before), it is considered the same cyclone. If not, it is considered a separate cyclone. Once an area has been searched, the searched sea level pressure values are masked out. Different methods (e.g., [36] and subsequent papers) use 850 hPa relative vorticity maxima for cyclone identification, but we chose minimum sea level pressure in part to gauge the surface cyclone response to nudging the full-atomosphere, above the boundary layer only, and above the troposphere only. The 1200 km radius is chosen to identify features characteristic of sizes expected to be influenced by the boundary layer.

2.4 Tropospheric Polar Vortex Identification

The tropospheric polar vortices were identified using the methods outlined in [11]. The potential temperature is calculated on a 2PVU (PVU=$1 \times 10^{-6}\mathrm{m}^2\mathrm{s}^{-1}\mathrm{Kkg}^{-1}$) surface (using [37]), and vortices are taken to be more than 2 standard deviations below domain mean. We use Ertel's potential vorticity in pressure coordinates, and potential temperature is interpolated onto the 2PVU surface. Ertel's potential vorticity equation is expressed as

$$\Pi = \frac{1}{\rho}\omega_a \cdot \nabla\theta, \tag{2.2}$$

where ρ is density, ω_a is absolute vorticity, and θ is potential temperature.

2.5 *Eady Growth Rate Calculation*

The Eady growth rate is expressed as

$$EGR = 0.3098\frac{|f||\frac{\partial u(z)}{\partial z}|}{N}. \tag{2.3}$$

The Eady growth rate (EGR) is a function of the Coriolis parameter f, the Brunt-Väisälä frequency $N = (\frac{g}{\theta}\frac{\partial\theta}{\partial z})^{1/2}$, and the gradient of the zonal wind $\frac{\partial u(z)}{\partial z}$. We used the methods outlined in [16, 38] to calculate the EGR at 500 hPa. The EGR at 500 hPa should be representative of the maximum baroclinicity of the storm because it is influenced by both upper and lower levels [16, 39]. The EGR is calculated in pressure coordinates by using the 400, 500, and 600 hPa levels. The maximum is considered to be the maximum mean of 500 km around the cyclone center during cyclone evolution. While one could use the relative vorticity to evaluate baroclinicity, the EGR takes into consideration both wind shear and thermodynamic buoyancy providing a better measure of baroclinicity.

2.6 *Cyclone Centered Approach*

Case studies allow for analysis of physical processes occurring during the evolution of the cyclone. We picked a case study over the Arctic Ocean that had reached a minimum sea level pressure under 975 hPa during its lifetime. For the cyclone case study, points within a great circle distance of 1200 km of cyclone centers were mapped with respect to standard cardinal direction. While some previous studies (eg. [23]) used a storm-rotated approach, our case studies indicated an east-west asymmetry that made most sense to use a cardinal direction approach similar to [10]. Horizontal cross sections were interpolated in bins of 50 km by 50 km distance from the center with the cyclone center coordinate at (0,0). Vertical cross sections were taken at the y=0 line of distance from the cyclone center.

2.7 Cyclone Compositing

Summer cyclone anomaly fields were calculated using a running mean 10 days before to 10 days after the time being composited. A running mean allows for an updated background state of the environmental conditions around the time of cyclone passage. Summer cyclones were composited during two life cycle stages. The first at the maximum EGR, and the second at the minimum sea level pressure. While previous studies have used fixed time intervals before and after the minimum sea level pressure, by looking at the maximum growth rate, we can constrain the cyclones to the same point in their life cycle as cyclone intensification rates can vary. At maximum EGR, composites are separated into warm core and cold core cyclones. Warm core cyclones are defined using the temperature anomalies at 850 hPa. If the inner 500 km around the center of the cyclone is warmer than the outer ring between 500 km and 1200 km and the anomaly at the cyclone center is positive, the cyclone is classified as a warm core cyclone. Otherwise, the cyclone is classified as a cold core cyclone. This methodology tests the hypothesis that warm and cold core cyclones have different structures without converting to phase space as in [21, 22].

Chapter 3
RESULTS

3.1 ERA5 Statistical Comparison

Before utilizing the model runs to examine Arctic cyclones, we first compared the output to ERA5 for the entire study period of May-September 2022. The hourly root mean squared error (RMSE) compared to ERA5 for sea level pressure, skin surface temperature, and 10 m wind speed are shown in Figure 3.1. RMSEs are computed directly from the CESM and ERA5 output (i.e. not anomalies). The RMSEs are higher for the ABL run for sea level pressure, skin surface temperature, and 10 m wind speed, which is expected because the run was nudged at fewer levels and not in the boundary layer. There is still decent agreement with ERA5 in the ABL run in terms of sea level pressure and 10 m wind speed with most values under 3 hPa and 3 m/s respectively. However, there is a noticeable difference of over 5 K in skin surface temperatures over land for both FA and ABL runs. This could be due to the different land parameterizations as well as the grid resolution of ERA5 (originally 0.25°x0.25°) and the model runs.

The hourly bias compared to ERA5 for sea level pressure, skin surface temperature, and 10 m wind speed are shown in Figure 3.2. The surface wind biases for both FA and ABL and sea level pressure bias for FA are small with magnitudes under 2 m/s and 2 hPa respectively. For the ABL run, there is a high sea level pressure bias over the Arctic Ocean, North America, and western Russia with magnitudes upwards of 2 hPa (Figure 3.2d). There is a low pressure bias of similar magnitude over Greenland and eastern Russia (Figure 3.2d). For skin surface temperature in both the FA and

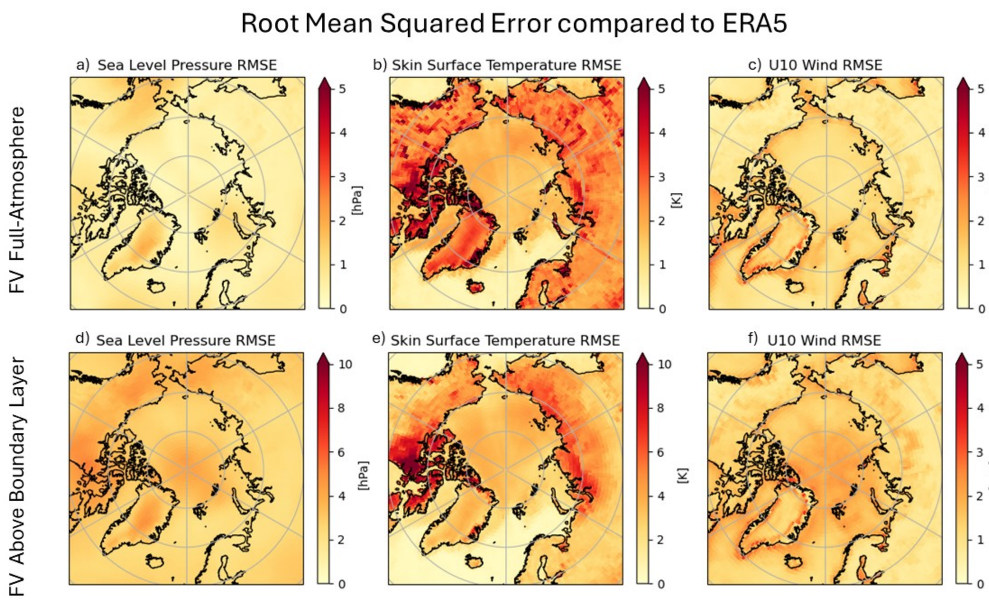

Figure 3.1: Root Mean Squared Error (RMSE) compared to ERA5 for the full-atmosphere run (a-c) and the above the boundary layer run (d-f) of sea level pressure (a,d), skin surface temperature (b,e), and 10 meter wind speed (c,f).

ABL runs, there is a high temperature bias of around 2 K over land and a cool bias along the Arctic frontal zone (coastline) and over the Arctic Ocean. The cool bias is much more pronounced in the ABL run (Figure 3.2e) with magnitudes upwards of 5 K. These larger biases in skin surface temperature could again be due to differences in land paramterizations and grid resolutions between ERA5 and the model runs, but should be considered in subsequent analysis.

Once we had taken note of the biases of the model runs compared to ERA5 over the study period, we ran the cyclone tracking algorithm on ERA5 regridded to 1° resolution and all three model runs. The frequency of cyclone center locations in ERA5 and the FA and ABL runs are shown in Figure 3.3. The locations are very similar between ERA5 and the FA run confirming the algorithm is working as

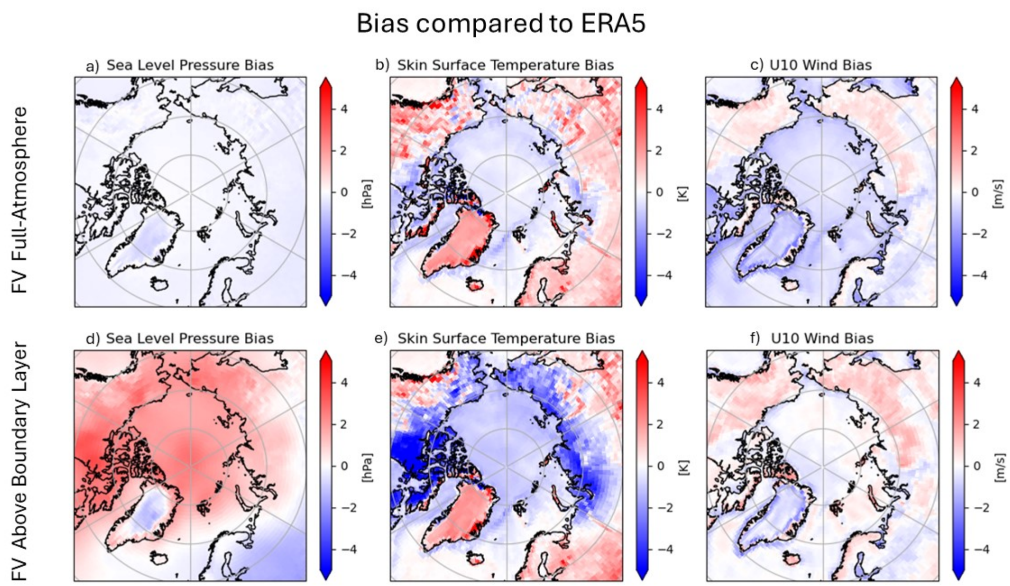

Figure 3.2: Bias compared to ERA5 for the full-atmosphere run (a-c) and the above the boundary layer run (d-f) of sea level pressure (a,d), skin surface temperature (b,e), and 10 meter wind speed (c,f).

intended. The cyclone center locations for the ABL run are similar to ERA5 except over the central Arctic Ocean (higher latitudes). Cyclones are more frequent in lower latitudes with the highest frequencies north east of Iceland, eastern Canada, and western Russia for ERA5 and both the FA, and ABL runs. The sea level pressures for all ERA5 cyclone centers most frequently fall between 990 and 995 hPa with the majority of cyclone centers between 985 and 995 hPa (Figure 3.4a). Sea level pressures for the FA (Figure 3.4b) run and the ABL run (Figure 3.4c) cyclone centers also most frequently fall between 990 and 995 hPa. However, there are fewer cyclone centers with sea level pressures between 985 and 990 hPa and more cyclone centers greater than 995 hPa in the ABL run. This could be due to the high pressure bias in Figure 3.2d. The sea level pressure range for centers of greater than 965 hPa and

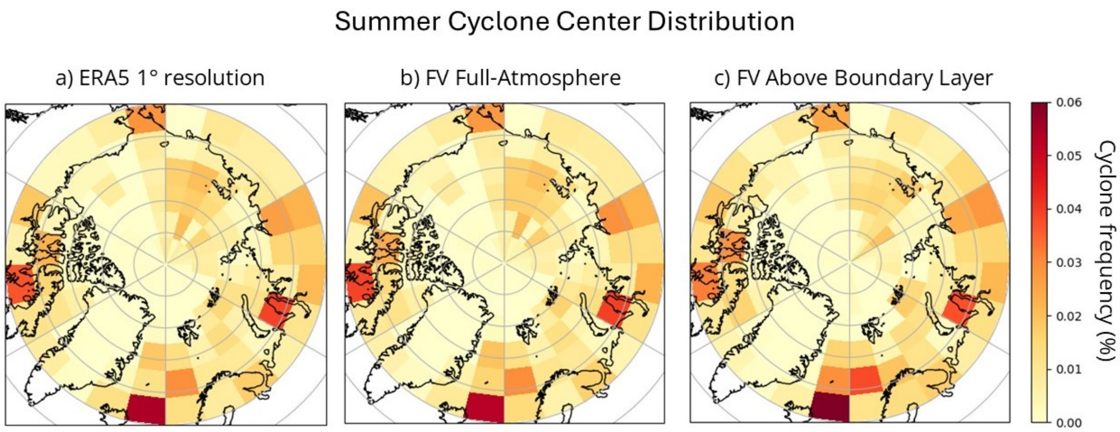

Figure 3.3: Frequency of cyclone centers present in Arctic regions over the study period of May-September 2022 for a) ERA5 b) the full-atmosphere run c) the above the boundary layer run.

less than 1010 hPa is the same for ERA5 (Figure 3.4a) and the ABL run (Figure 3.4c). The FA run (Figure 3.4b) has a similar minimum range, but does not have cyclone-center sea-level pressures above 1005 hPa. Small biases in surface variables and cyclone center location and sea level pressure distribution suggest the model can simulate the summer 2022 study period well enough to proceed with a realistic case study and composite analysis.

3.2 Cyclone Case Study

The cyclone track and minimum sea level pressure time-series are shown in Figure 3.5 for ERA5 1° resolution and the FA, ABL, and AT runs. In ERA5 and all three model runs, the cyclone forms over mountains in Russia, crosses the Arctic frontal zone, and spends time in the Arctic ocean before dissipation (Figure 3.4a). The tracks for ERA5 and the FA run are very similar in terms of starting location, ending location, and track. The ABL run cyclone starts about 5° farther north, but overall follows a

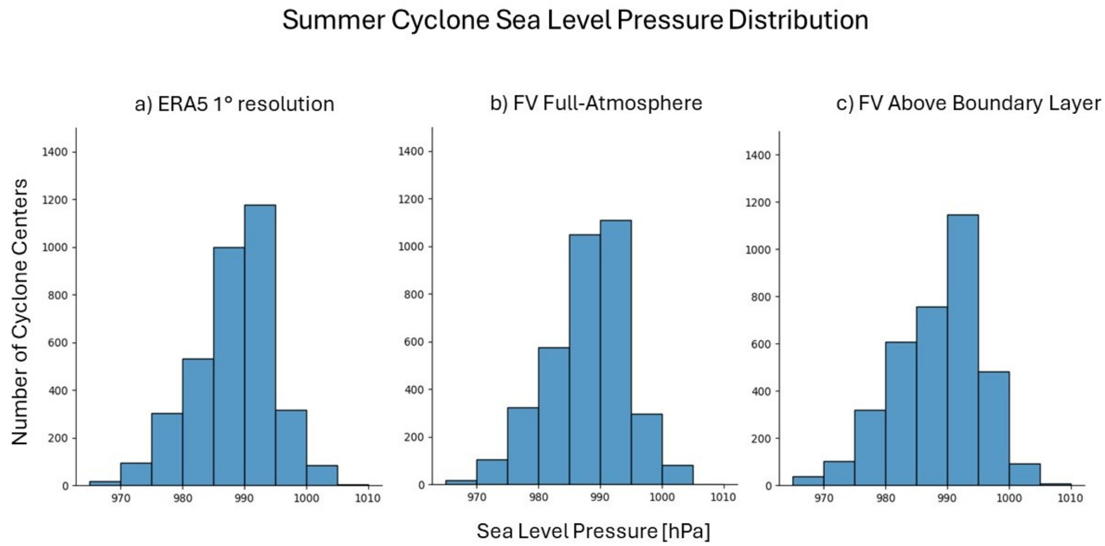

Figure 3.4: Cyclone center sea level pressure distribution for a) ERA5, b) the full-atmosphere run, and c) the above the boundary layer run during the study period of May-September 2022

similar track for the remainder of the storm's lifetime. The AT run cyclone starts west of ERA5 and the other runs, but crosses the Arctic frontal zone in the same area. As the cyclone in the AT run enters the Arctic ocean, it stays east of the other tracks and doesn't propagate as far north. This latitudional propagation bias in GCMs has been noted in previous studies [25, 35, 26]. Nudging does improve this bias for the ABL and FA runs. The ERA5 and the FA run have very similar sea level pressure time series starting on 07/03/2022 at 994 hPa and reaching sea level pressures under 975 hPa on 07/06/2022 and 07/07/2022. There is a slight increase in sea level pressure of 4 hPa for the ERA5 cyclone and 3 hPa for the FA run cyclone on 07/06/2022 before decreasing again to around 973 hPa. The ABL run cyclone starts after the ERA5 and the FA run cyclones on 07/03/2022 at around 992 hPa and reaches sea level pressures under 970 hPa on both 07/06/2022 and 07/07/2022. There is no increase in sea level

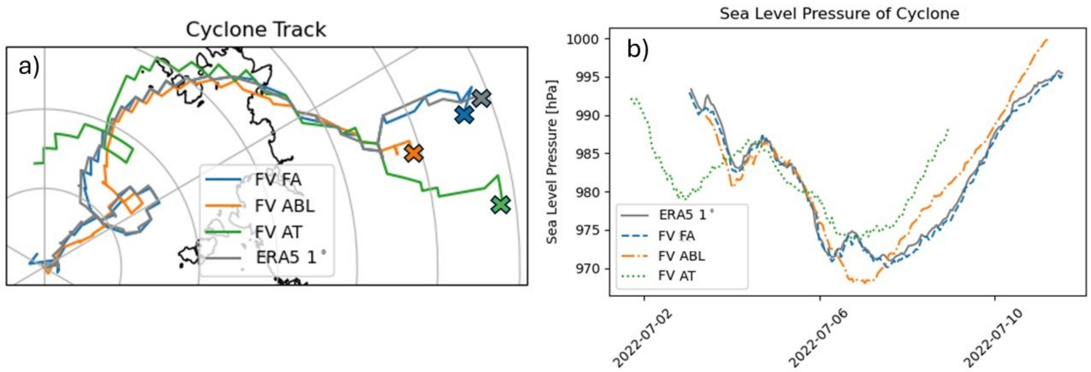

Figure 3.5: a) Cyclone track for ERA5 1° (gray), the full-atmosphere run (blue), the above the boundary layer run (orange), the above the troposphere run (green). The start of the tracks is marked by an x. b) Time series of minimum sea level pressure over the cyclone lifetime for ERA5 1° (gray), the full-atmosphere run (blue), the above the boundary layer run (orange), the above the troposphere run (green).

pressure on 07/06/2022 as in ERA5 and the FA run. The AT run cyclone starts earlier than the rest during the night of 07/01/2022 and ends earlier by about 2 days. The AT cyclone has the shallowest minimum sea level pressure of the 3 model runs at 975 hPa.

The cyclone case study was further analyzed in the context of the two sources of baroclinicity. The first being the crossing of the Arctic frontal zone, and the second being the interaction with a TPV. Maps of potential temperature on the 2 PVU surface at 21:00 on 07/04/2022 are shown in Figure 3.6a for the FA run and 3.6b for the ABL run. The map of potential temperature on the 2 PVU surface at 09:00 on 07/04/2022 is shown in 3.6c for the AT run. For all runs, the cyclone center is just past the coastline indicating the cyclone is crossing the Arctic frontal zone. There is not a TPV near the cyclone yet in either run, but a TPV is present near the pole. The TPV is characterized by potential temperature under 290 K in a small region above 85° N and north of Russia. A time series of the 500 hPa EGR is shown in

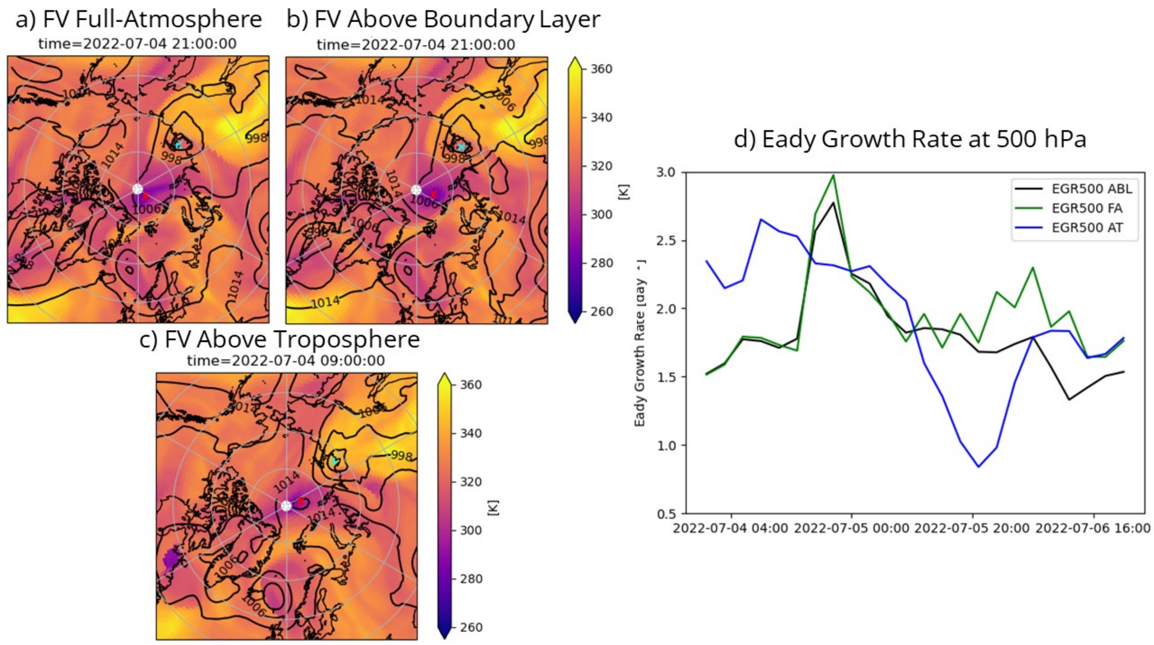

Figure 3.6: a) and b) Maps of potential temperature on the 2PVU surface at 21:00 on 07/04/2022 for the full atmosphere run (a) and the above the boundary layer run (b). c) Map of potential temperature on the 2PVU surface at 09:00 on 07/04/2022 for the above troposphere run. The black contours are sea level pressure and the cyan x marks the cyclone center. The red x marks the location of the TPV. d) A time series of Eady growth rate at 500 hPa for the cyclone.

Figure3.6d. As the cyclone crosses the Arctic frontal zone in all three runs, the 500 hPa EGR peaks. The EGR peaks at just under 3 day^{-1} for the FA run and just above 2.75 day^{-1} for the ABL run, and just under 2.75 day^{-1} for the AT run. This indicates the maximum generation of baroclinicity was driven by the crossing of the Arctic frontal zone for this cyclone. By 21:00 on 07/06/2022, a TPV had interacted with the cyclone in all three runs, which is evident in Figure 3.7. The cyclone centers for the FA (Figure 3.7a) and ABL (Figure 3.7b) runs have propagated further from the coastline and have interacted with the TPV that was also present in Figure 3.6a,b. For the AT run, the cyclone and TPV are farther south and the sea level pressure

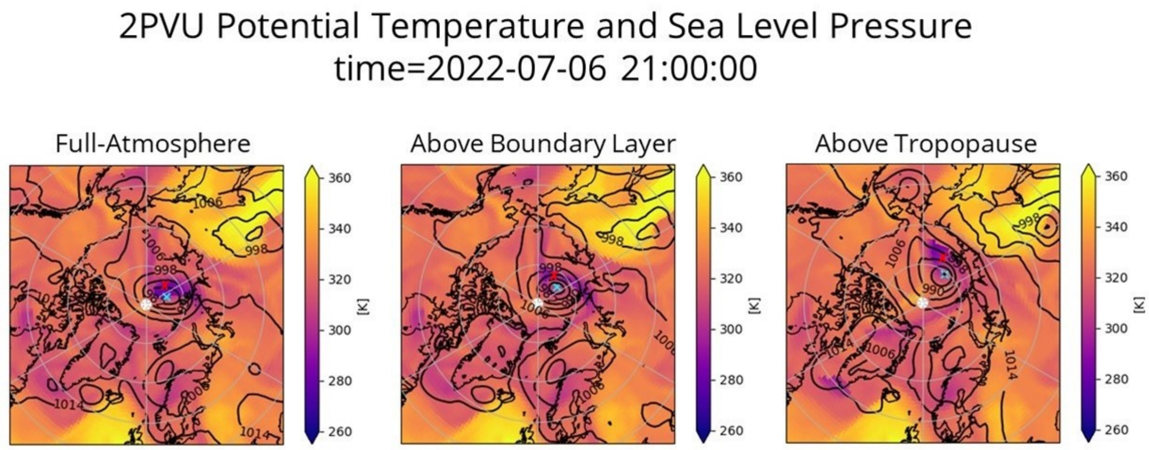

Figure 3.7: Maps of potential temperature on the 2PVU surface at 21:00 on 07/06/2022 for the full atmosphere run (a), the above the boundary layer run (b), and the above the troposphere run (c). This figure is formatted similarly to Figure 3.6a,b. The black contours are sea level pressure and the cyan x marks the cyclone center. The red x marks the location of the TPV.

gradient is not as large (Figure 3.7c).

3.2.1 Thermodynamic Evolution

Using a storm centered approach, we explored the thermodynamic evolution in terms of 850 hPa temperature and total precipitable water from maximum sea level pressure to storm maturation (minimum sea level pressure for the ABL run). To keep the timing across all analyses, we used the maximum EGR for the FA and ABL runs. During this time, the EGR is still relatively large for the AT run. At maximum EGR, or 21:00 on 07/04/2022, ERA5 and all three model runs have very warm 850 hPa temperatures above 285K in the southern part of the storm (Figure 3.8a-d). In addition there is moisture associated with the warm sector with total precipitable water values above 30 kg/m^2 in ERA5 (Figure 3.8e) and above 40 kg/m^2 in the model runs (Figure 3.8f-h). As the models are less and less constrained by nudging,

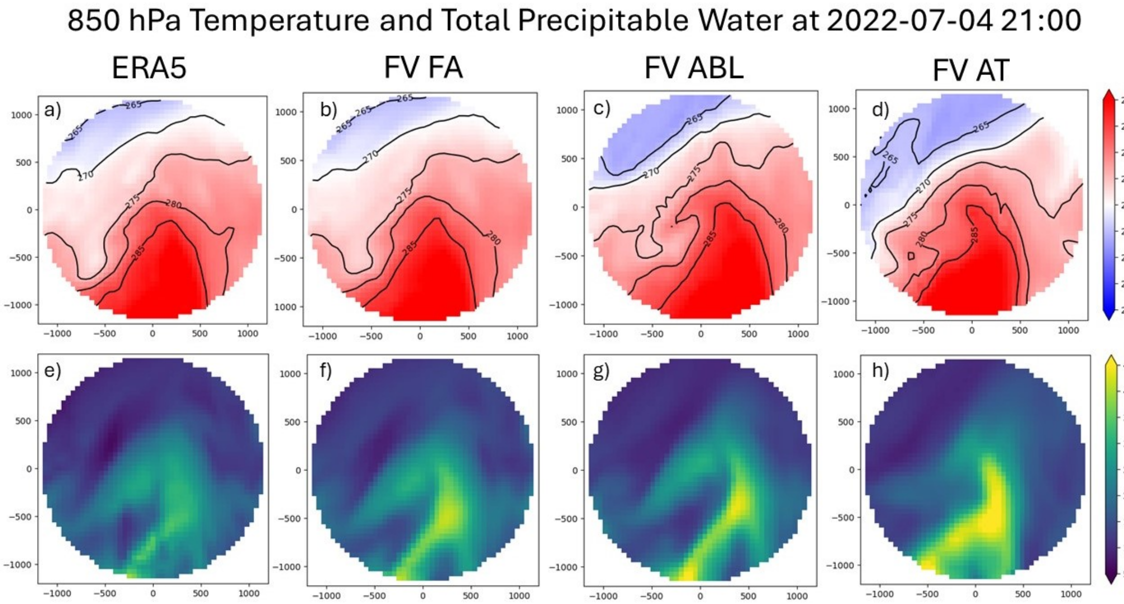

Figure 3.8: 850 hPa temperature (a-d) and total precipitable water (e-h) for ERA5 (a,e), the full-atmosphere run (b,f), the above the boundary layer run (c,g), and the above the troposphere run (d,h) at 21:00 on 07/04/2022. This is a storm centered approach where coordinate 0,0 is the center of the storm. Cardinal North is upwards.

the amount of moisture increases in this storm with values greater than 45 kg/m^2 in both ABL (Figure 3.8g) and AT (Figure 3.8h) runs. The warm, moist nature of the cyclone indicates it is a warm core storm at maximum EGR. At 21:00 on 07/05/2022, 24 hours later, the 850 hPa temperatures have decreased overall with the coldest temperatures north west of center in ERA5 and all model runs (Figure 3.9a-d). This cold sector has temperatures around 268 K for ERA5 and the FA run, 265 K for the ABL run, and 265 K for the AT run. The cold sector is largest in the ABL run and smallest in the FA run. The warm sector values are above 275 K in ERA5 and all model runs. As cold air intrudes, the cyclone has an east-west asymmetry seen in [10], and the cyclone gets drier. The maximum total precipitable water values are all under 30 kg/m^2 and values largely under 10 kg/m^2 corresponding to the cold sectors. The

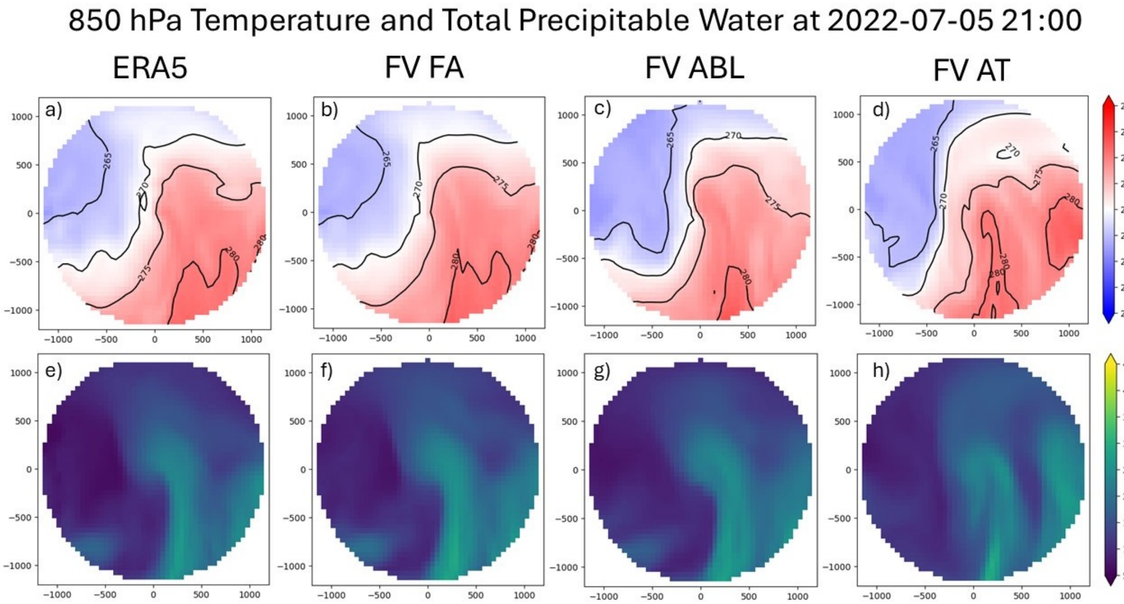

Figure 3.9: As in 3.8 for 21:00 on 07/05/2022.

AT run is not co-located (farther south) and is nudged less, which might contribute to the difference in temperature and moisture profiles. At 21:00 on 07/06/2022, the cold sector has occluded the warm sector from the center of the storm in ERA5, the FA run, and the ABL run (Figure 3.10). Magnitudes of those cold sectors are slightly lower than in Figure 3.9 with a larger swath of temperatures under 265K. Because the cyclone centers are relatively close to the pole,the area north of the cyclone centers is reduced in Figure 3.13a-c. The AT run does not have occlusion to the same degree, which could be due to the location of the cyclone and the delayed interaction with the TPV (we will elaborate in 3.2.2). The cold core cyclone in ERA5, the FA run, and the ABL run is also very dry in the storm center with values largely under 10 kg/m^2. The AT run has a similar dry sector in magnitude corresponding the cold sector. A cold core cyclone at maturation is consistent with previous studies [17, 22, 23].

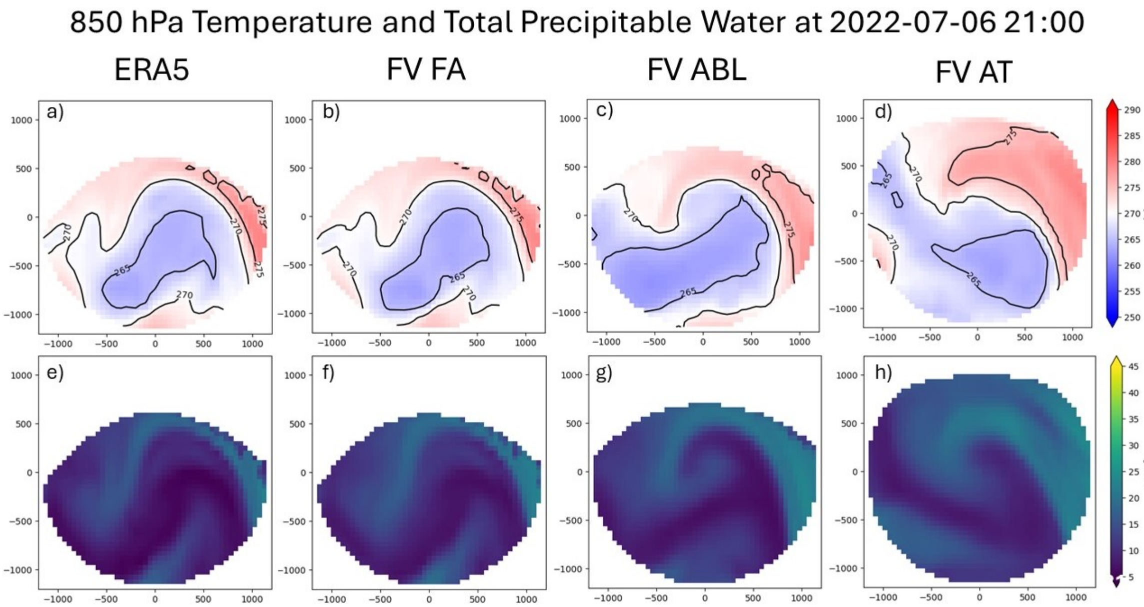

Figure 3.10: As in 3.8 for 21:00 on 07/06/2022. Since cardinal North is upwards, as the cyclone gets closer to the pole, the distance from the center of the cyclone to the pole is less than 1200 km.

3.2.2 Dynamic Evolution

In addition to the thermodynamic evolution of the cyclone, we examined the dynamic evolution in terms of the 10 m wind speed, sea level pressure, and 500 hPa vertical velocity. At 21:00 on 07/04/2022 or maximum EGR, the sea level pressure minimums (greater than 985 hPa) are not very low compared to the minimum sea level pressures reached over the evolution of the cyclone (Figure 3.11a-d). The cyclone sea level pressure contours are asymmetric in ERA5 and all model runs with lower pressures extending farther south. The 10 m wind speeds are relatively weak for ERA5 and the FA run with maximums just over 10 m/s. The ABL and AT runs have higher maximum wind speeds of around 13 m/s. The 500 hPa vertical velocity shows updrafts related to warm sector in Figure 3.11e-g. The updrafts are strongest in ERA5 with

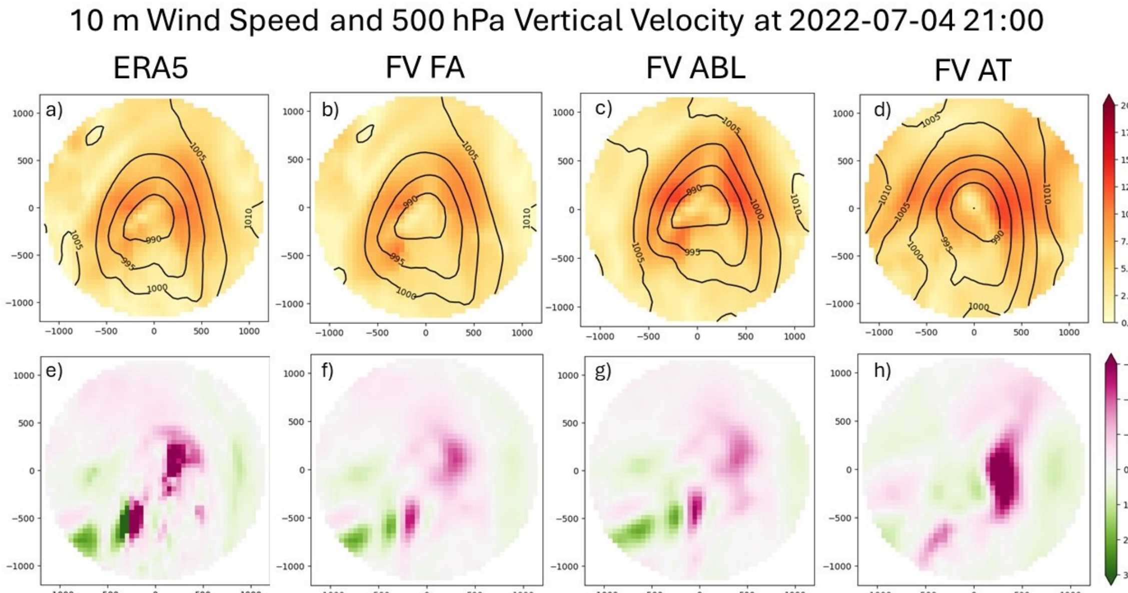

Figure 3.11: 10 m wind speed with sea level pressure contours (a-d) and 500 hPa vertical velocity (e-h) for ERA5 (a,e), the full-atmosphere run (b,f), the above the boundary layer run (c,g), and the above the troposphere run (d,h) at 21:00 on 07/04/2022. The vertical velocity is in pressure units, so negative values indicate upward motion.

values of -30 hPa/hour. The updrafts are weaker in the FA and ABL runs by about 10 hPa/hour. The AT run has a very strong updraft over the warm sector, which could be because of the difference in vertical structure. This will be further explored in section 3.2.3. The updrafts could be enhanced by crossing the Arctic frontal zone because the surface low is strengthened with the strengthening of the surface pressure gradient. In addition, surface friction in the boundary layer enhances surface convergence, which is especially important in lower-level dominated storms.The downdrafts in the south western region could be related to a cold front ahead of the cold air intrusion. At 21:00 on 07/05/2022, the surface cyclone is deeper with sea level pressures under 980 hPa, contours closer together, and higher 10 m wind speeds over 15 m/s (Figure 3.12a-d). The cyclone is more axisymmetric in all panels, and the wind speeds are higher in

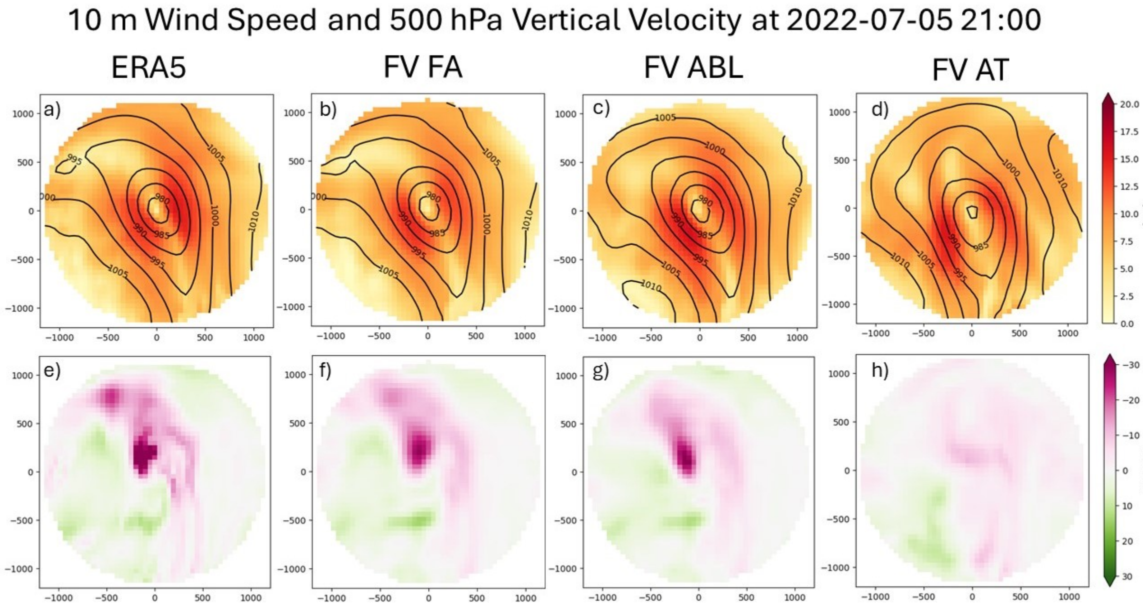

Figure 3.12: As in 3.11 for 21:00 on 07/05/2022.

the ABL and AT runs than ERA5. The 500 hPa vertical velocity showcases the TPV interaction in ERA5, and the FA and ABL runs with the high values of -30 hPa/hour north west of storm center(Figure 3.12e-g). The AT run is not co-located with the TPV yet (Figure 3.12h). At maturation or, 21:00 on 07/06/2022, the 10 m winds are axisymetric for ERA5 and the FA and ABL runs (Figure 3.13a-c). The surface cyclone is deeper for the ABL run than ERA5, and the ABL run has the highest wind speeds of around 20 m/s. The updrafts and downdrafts are not as strong at maturation (Figure 3.13e-h). An axisymmetric storm is in-line with the cyclone being a cold core cyclone.

3.2.3 Vertical Cross-sections

We analyzed vertical cross-sections to investigate the 3-D evolution of the cyclone. The cross-sections are west to east cross-sections at the y=0 line in Figures 3.11

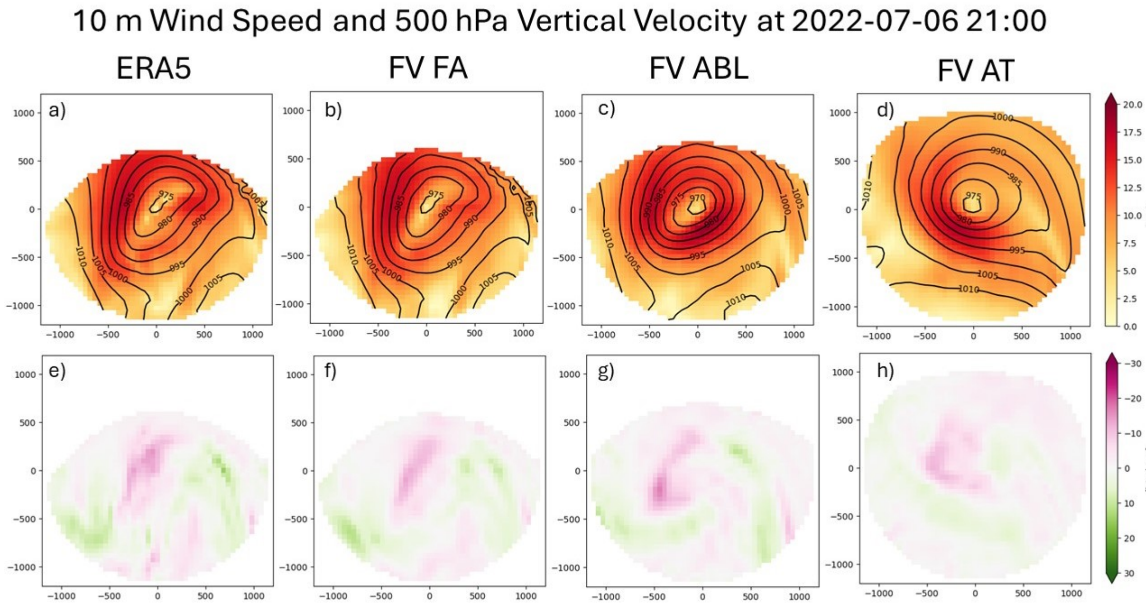

Figure 3.13: As in 3.11 for 21:00 on 07/06/2022.

and 3.13. The meridional wind speed (southerly wind positive) at 07/04/2022, or maximum EGR, is shown in Figure 3.14. The gray contours are potential temperature, the solid black contour is the dynamic tropopause (2PVU surface), and the dotted black line is the PBL height. In ERA5 and all three model simulations, the cyclonic circulation is baroclinic (titled with height), though it does not extend throughout the profile. Instead, it is mostly confined to the lower levels. The largest portion of the cyclonic rotation (northerly on the left and southerly winds on the right) is from the surface to 6 km above mean sea level for ERA5 and the FA and ABL model runs. The baroclinic cyclonic circulation in the AT run does not extend above 4 km. Thus, the circulation is most strongly influenced by lower levels, or more specifically, the crossing of the Arctic frontal zone. The dynamic tropopause is relatively high, which is expected since there is no TPV present. The lower level wind speeds are higher in ERA5 and the AT run, which would correspond with the higher 500 hPa vertical

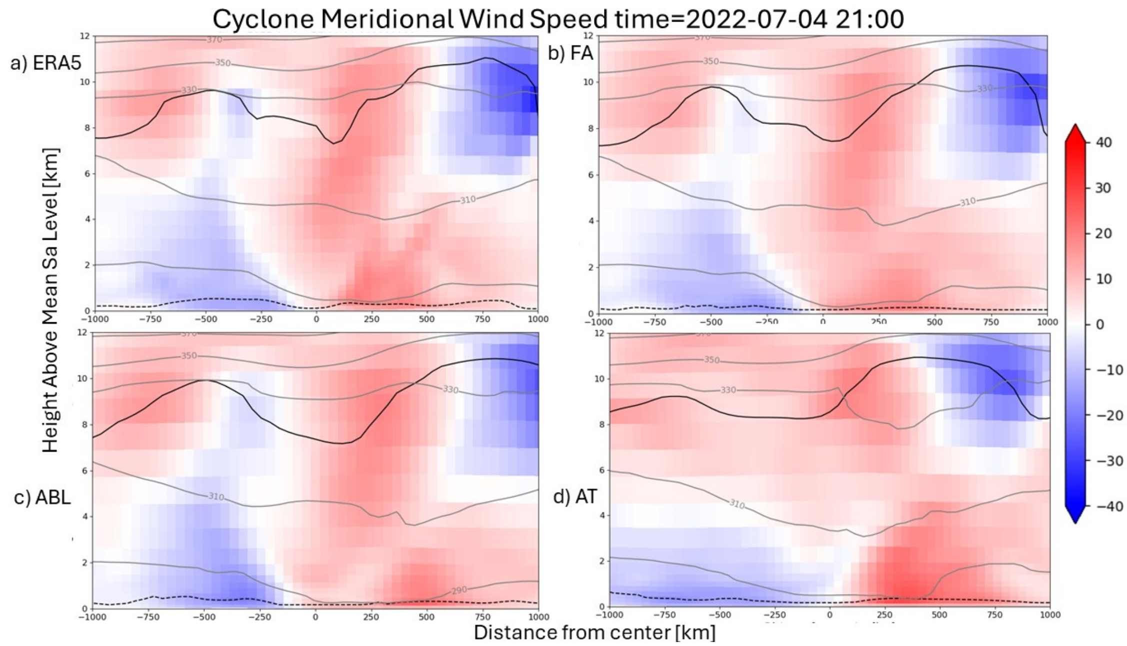

Figure 3.14: West to East cross-sections of meridional wind speed for a) ERA5, b) the full-atmosphere run, c) the above the boundary layer run, and d) the above the troposphere run at 21:00 on 07/04/2022. The gray contours are potential temperature in K. The black line is the dynamic tropopause at the 2PVU surface, and the black dotted line is the planetary boundary layer height.

velocities in Figure 3.11. The vertical wind structure in the AT run is different with northerly meridional wind speeds at the center of the cyclone and extending upward for 2 km, so the circulation is more centered at the location of the warm sector. Thus, leading to larger updrafts. At 21:00 on 07/06/2022, once the cyclone had interacted with a TPV, the meridional wind speeds are much stronger (Figure 3.15). The maximum meridional wind speed magnitudes are doubled at 40 m/s compared to 20 m/s at maximum EGR. The highest wind speeds are also located at the mid and high levels instead of near the surface. The dynamic tropopause has lowered by at least 4 km, the boundary layer height has increased (more so in ERA5), and tight

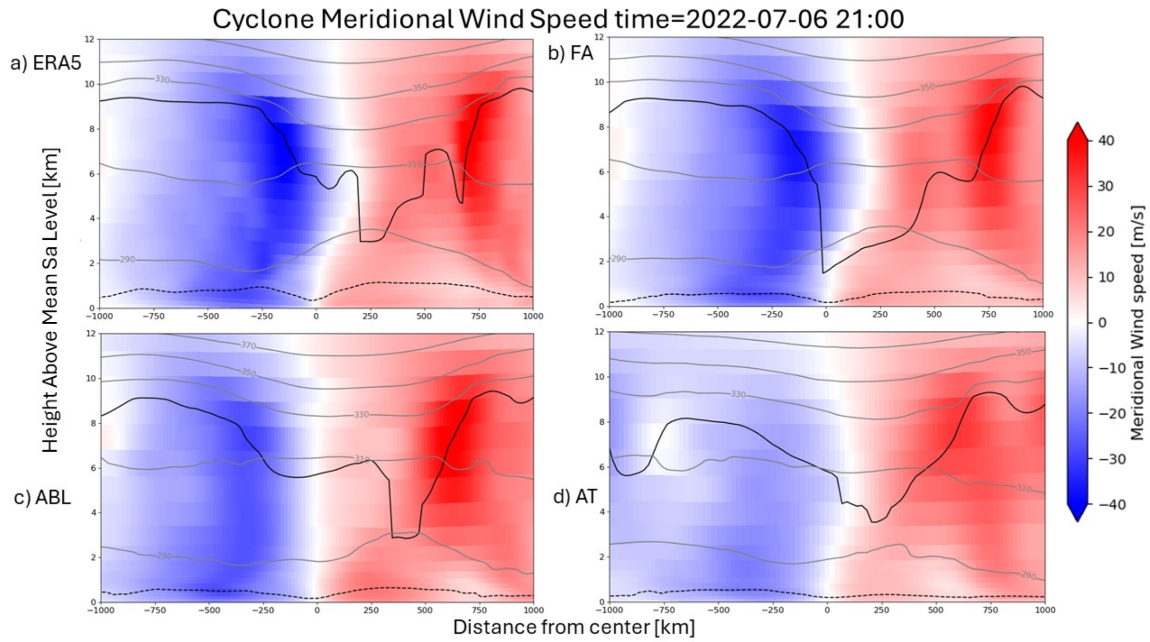

Figure 3.15: As in 3.14 for 21:00 on 07/06/2022.

potential temperature contours are intruding from the stratosphere. The cyclone in ERA5 and all model runs is a very well defined nearly axisymmetric, barotropic storm similar to previous studies [17].

3.3 Composites

While cases studies are important to discern physical processes affecting cyclone structure and evolution, they may not be representative of most cyclones. Here, we investigate the composite structure of the 850 hPa temperature in Figure 3.16 and 10 m wind speed in Figure 3.17. Warm core and cold core cyclones had distinct thermodynamic structures at maximum EGR in both the FA and ABL runs. The warm core storms had positive anomalies in the center and south east quadrant of the cyclone and negative anomalies elsewhere. The cold core storms had cold anomalies in the

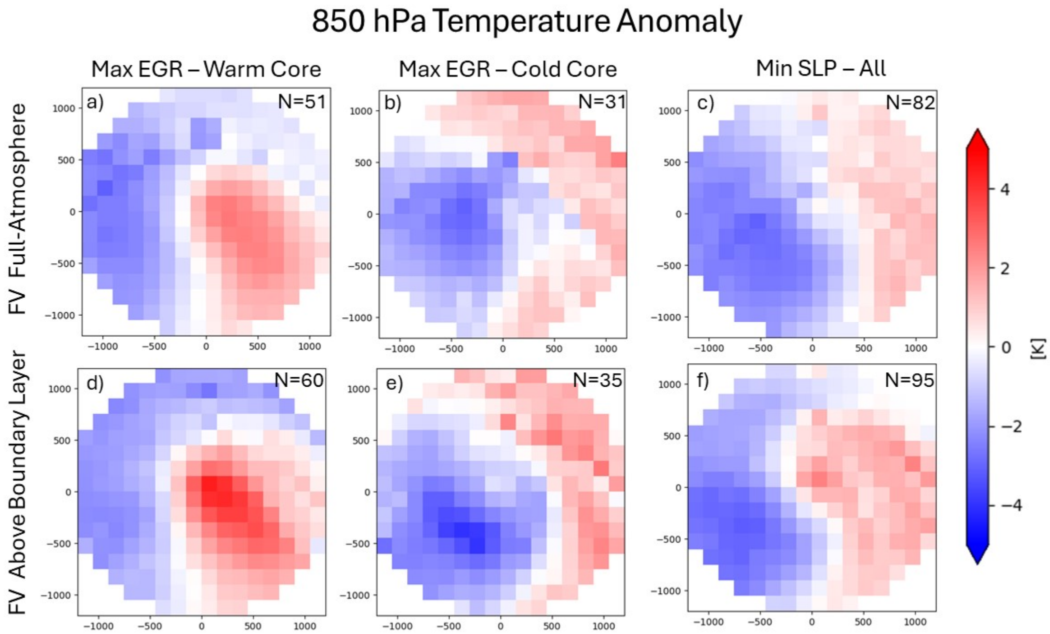

Figure 3.16: 850 hPa temperature anomalies for the full-atmosphere run (a-c) and the above the boundary layer run (d-f) for warm core storms at maximum Eady growth rate (a,d), cold core storms at maximum Eady growth rate (b,e), and all storms at minimum sea level pressure (c,f).

center and the south western section of the storm and positive anomalies elsewhere. The anomalies were larger in the ABL run with magnitudes upwards of 4 K. In both model runs, there were more warm core storms than cold core storms. When all storms are combined at minimum sea level pressure, there is a cold anomaly on the western side and a warm anomaly on the eastern side similar to the findings in [10]. Again, the anomalies are larger in the ABL run. In terms of the surface wind anomalies, the winds are stronger in the warm sector for warm core storms and in the cold sector for cold core storms in both model runs (Figure 3.17a,b,d,e). The 10 m wind speed anomalies are 2 m/s larger and more asymmetric for the ABL run at maximum EGR. All storms at minimum sea level pressure have more axisymetric winds around

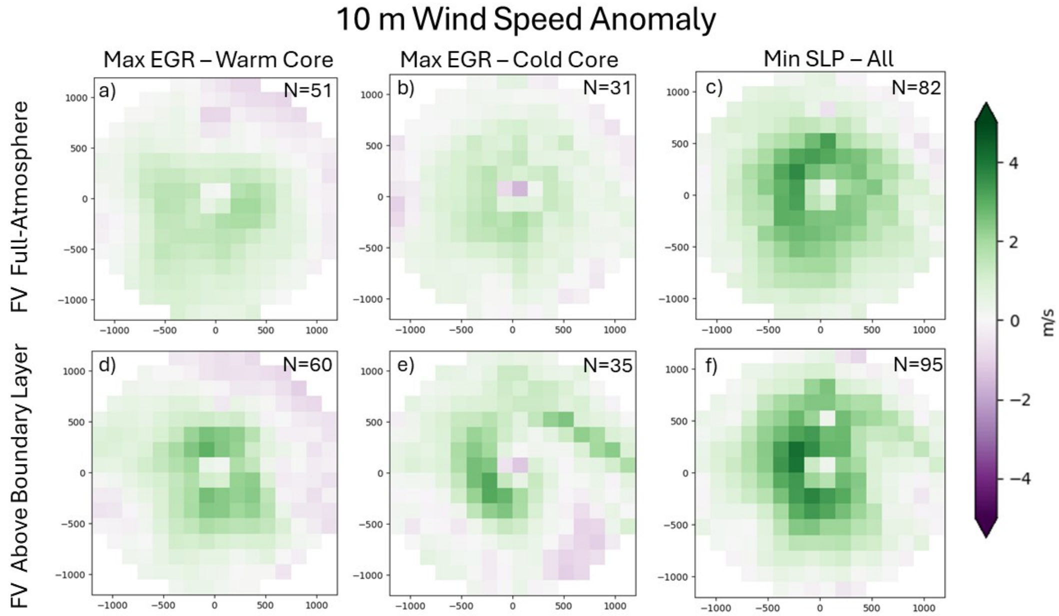

Figure 3.17: 10 m wind speed anomalies for the full-atmosphere run (a-c) and the above the boundary layer run (d-f) for warm core storms at maximum Eady growth rate (a,d), cold core storms at maximum Eady growth rate (b,e), and all storms at minimum sea level pressure (c,f).

the cyclone center indicative of a mature summer Arctic cyclone.

Chapter 4
DISCUSSION

Despite recent progress on the topic, the structure and evolution of summer Arctic cyclones has not fully been determined. The first model of an Arctic cyclone presented in [17] showcased an axisymmetric storm with a warm stratosphere and cold troposphere that is 5000 km in size. However, an analysis of multiple cyclones revealed an asymmetric thermodynamic structure with cold, dry air to the west and warm dry air to the east [10]. The authors in [10] did not take into consideration cyclone life cycle. Studies that have examined the evolution of Arctic cyclones have shown that Arctic cyclones can be baroclinic and barotropic in nature depending on the stage of evolution and the main source of vorticity [15, 21, 23, 22].

Our study found that utilizing a nudging technique, atmosphere-only simulations in CESM were able to reproduce cyclone location (Figure 3.3) and sea level pressures (Figure 3.4) found in ERA5 over the course of the study period and a cyclone case study examined in section 3.2. All model simulations had the same cyclone intensify over the Arctic frontal zone with a warm core at maximum EGR and interact with a TPV before maturation. The FA and ABL runs had a cold core at minimum sea level pressure. This evolution from warm core to cold core is consistent with case studies that intensify over the Arctic frontal zone without a TPV initially present [21, 22]. The 500 hPa vertical velocities and meridional wind profiles show the storm intensification with TPV interaction in ERA5 and the FA and ABL runs. In addition, the cyclone in ERA5 and all three model runs exhibited the transition from a baroclinic storm before TPV interaction to a barotropic storm after TPV interaction. This supports the hypothesis that the vertical structure of the Arctic cyclone is determined by the main source of vorticity. A composite analysis in section 3.3 showed warm core and cold core cyclones had distinct thermodynamic and dynamic structures at maximum EGR, but combining all cyclones led to a east/west thermal asymmetry as noted in [10, 24]. However, this might not be entirely representative of cyclone structure given the physical processes that govern cold core and warm core cyclones are different. By understanding that surface generation of baroclincity near the Arctic frontal zone governs many warm core storms and TPVs are generally associated with cold core storms, it would be important to analyze them separately. Although, the definition of warm core versus cold core used in this study is quite simplistic, and the separation is not always clear. This is why certain points that are important to cyclone evolution such as maximum EGR and minimum sea level pressure are used in this study.

Further analyzing model bias, the intensity of the surface winds and moisture profile are greater in the ABL and AT runs than ERA5, and the planetary boundary layer height (PBLH) and tropopause height are different in ERA5 compared to CESM. The differences in planetary boundary layer height and surface variables are most likely due to the different boundary layer schemes as CLUBB is a statistical scheme and struggles with deep convection. The specific humidity was not nudged in this study, so the difference in total precipitable water is also due to the difference in micro-physics schemes. An important next step would be to compare to observations, as ERA5 has its own biases.

Chapter 5
CONCLUSIONS AND FUTURE WORK

In this study, we investigated the structure and evolution of Summer 2022 Arctic cyclones using CESM atmosphere-only simulations nudged to ERA5. We focused on three model experiments, full-atmosphere (FA), above the boundary layer only (ABL), and above the troposphere only (AT) to explore model biases compared to ERA5. We found the FA and ABL runs compared reasonably well to ERA5 in surface RMSE and bias, cyclone location, and cyclone minimum sea level pressure. Through a case study analysis, we focused on a warm core storm that was enhanced by the Arctic frontal zone interacted with a TPV before maturation in ERA5 and all model runs. The cyclone went from a warm core storm at maximum EGR to a cold core storm at maturation in ERA5 and the FA and ABL model runs. A warm core storm and lower-level dominant storm indicates boundary layer processes were important in the storm's development and evolution. Nudging only above the boundary layer, and to an extent nudging only above the troposphere, was able to capture this process. However, sea surface temperatures and sea ice extent were held constant, so the Arctic frontal zone's baroclinicity strength should be similar in all model runs. Since nudging above the troposphere produced a cyclone in the same region that also interacted with a TPV, it indicates that the upper-levels are still a significant source of baroclinicity and a main driver of cyclogensis. In a fully-coupled run, the constrain on the upper circulation might not be enough without the constraint on SSTs and sec ice extent. Through a composite analysis, we found that the warm core and cold core cyclones at maximum EGR have distinct 850 hPa temperature and 10 m wind speed anomalies, but combining cyclones at minimum sea level pressure led to similar composites in previous literature. The high biases in moisture and wind speeds in the ABL and AT runs are largely do to the different boundary layer and cloud physics parameterizations in ERA5 and CESM, so observational comparison is warranted to contextualize these results.

There are many future directions we can take this study. The first is to increase the sample size of the case studies and cyclones in our composites and compare our findings to observations in the area as ERA5 has its own model biases. The second is to explore the nudged ARCTIC grid simulation for the same study period to determine if grid resolution had an impact on our findings. Additionally, we would like to explore the effects of removing the TPV in the nudging dataset for our case study. Eventually, we would like to investigate the impacts of perturbing the model such as fully-coupling the model and improving the boundary layer parameterization on the structure and evolution of summer Arctic cyclones.

BIBLIOGRAPHY

[1] R. Davy and S. Outten, “The arctic surface climate in cmip6: Status and developments since cmip5,” *Journal of Climate*, vol. 33, no. 18, pp. 8047 – 8068, 2020.

[2] N. S. Steiner, J. Bowman, K. Campbell, M. Chierici, E. Eronen-Rasimus, M. Falardeau, H. Flores, A. Fransson, H. Herr, S. J. Insley, H. M. Kauko, D. Lannuzel, L. Loseto, A. Lynnes, A. Majewski, K. M. Meiners, L. A. Miller, L. N. Michel, S. Moreau, M. Nacke, D. Nomura, L. Tedesco, J. A. van Franeker, M. A. van Leeuwe, and P. Wongpan, “Climate change impacts on sea-ice ecosystems and associated ecosystem services,” *Elementa: Science of the Anthropocene*, vol. 9, p. 00007, 10 2021.

[3] A. Durkalec, C. Furgal, M. W. Skinner, and T. Sheldon, “Climate change influences on environment as a determinant of Indigenous health: Relationships to place, sea ice, and health in an Inuit community.,” *Social science & medicine (1982)*, vol. 136-137, pp. 17–26, July 2015. Place: England.

[4] R. Lei, D. Gui, J. K. Hutchings, P. Heil, and N. Li, “Annual cycles of sea ice motion and deformation derived from buoy measurements in the western arctic ocean over two ice seasons,” *Journal of Geophysical Research: Oceans*, vol. 125, no. 6, p. e2019JC015310, 2020. e2019JC015310 2019JC015310.

[5] J. Mortin, G. Svensson, R. G. Graversen, M.-L. Kapsch, J. C. Stroeve, and L. N. Boisvert, “Melt onset over arctic sea ice controlled by atmospheric moisture transport,” *Geophysical Research Letters*, vol. 43, no. 12, pp. 6636–6642, 2016.

[6] P. M. Finocchio, J. D. Doyle, and D. P. Stern, “Accelerated Sea Ice Loss from Late Summer Cyclones in the New Arctic,” *Journal of Climate*, vol. 35, pp. 7751–7769, Nov. 2022. Publisher: American Meteorological Society Section: Journal of Climate.

[7] M. G. Asplin, R. Galley, D. G. Barber, and S. Prinsenberg, “Fracture of summer perennial sea ice by ocean swell as a result of arctic storms,” *Journal of Geophysical Research: Oceans*, vol. 117, no. C6, 2012.

[8] J. Zhang, R. Lindsay, A. Schweiger, and M. Steele, "The impact of an intense summer cyclone on 2012 arctic sea ice retreat," *Geophysical Research Letters*, vol. 40, no. 4, pp. 720–726, 2013.

[9] E. Blanchard-Wrigglesworth, M. Webster, L. Boisvert, C. Parker, and C. Horvat, "Record arctic cyclone of january 2022: Characteristics, impacts, and predictability," *Journal of Geophysical Research: Atmospheres*, vol. 127, no. 21, p. e2022JD037161, 2022. e2022JD037161 2022JD037161.

[10] R. Clancy, C. M. Bitz, E. Blanchard-Wrigglesworth, M. C. McGraw, and S. M. Cavallo, "A cyclone-centered perspective on the drivers of asymmetric patterns in the atmosphere and sea ice during arctic cyclones," *Journal of Climate*, pp. 1 – 47, 2022.

[11] S. M. Cavallo and G. J. Hakim, "Composite Structure of Tropopause Polar Cyclones," *Monthly Weather Review*, vol. 138, pp. 3840–3857, Oct. 2010. Publisher: American Meteorological Society Section: Monthly Weather Review.

[12] S. M. Cavallo and G. J. Hakim, "Radiative impact on tropopause polar vortices over the arctic," *Monthly Weather Review*, vol. 140, no. 5, pp. 1683 – 1702, 2012.

[13] A. Yamagami, M. Matsueda, and H. L. Tanaka, "Extreme arctic cyclone in august 2016," *Atmospheric Science Letters*, vol. 18, no. 7, pp. 307–314, 2017.

[14] M. T. Bray and S. M. Cavallo, "Characteristics of long-track tropopause polar vortices," *Weather and Climate Dynamics*, vol. 3, pp. 251–278, Mar. 2022. Publisher: Copernicus GmbH.

[15] S. L. Gray, K. I. Hodges, J. L. Vautrey, and J. Methven, "The role of tropopause polar vortices in the intensification of summer Arctic cyclones," *Weather and Climate Dynamics*, vol. 2, no. 4, pp. 1303–1324, 2021.

[16] I. Simmonds and I. Rudeva, "The great arctic cyclone of august 2012," *Geophysical Research Letters*, vol. 39, no. 23, 2012.

[17] T. Aizawa and H. L. Tanaka, "Axisymmetric structure of the long lasting summer Arctic cyclones," *Polar Science*, vol. 10, no. 3, pp. 192–198, 2016.

[18] S. Peng, Q. Yang, M. D. Shupe, X. Xi, B. Han, D. Chen, S. Dahlke, and C. Liu, "The characteristics of atmospheric boundary layer height over the Arctic Ocean

during MOSAiC," *Atmospheric Chemistry and Physics*, vol. 23, pp. 8683–8703, Aug. 2023. Publisher: Copernicus GmbH.

[19] A. Crawford and M. Serreze, "A New Look at the Summer Arctic Frontal Zone," *Journal of Climate*, vol. 28, pp. 737–754, Jan. 2015. Publisher: American Meteorological Society Section: Journal of Climate.

[20] A. D. Crawford and M. C. Serreze, "Projected Changes in the Arctic Frontal Zone and Summer Arctic Cyclone Activity in the CESM Large Ensemble," *Journal of Climate*, vol. 30, pp. 9847–9869, Dec. 2017. Publisher: American Meteorological Society Section: Journal of Climate.

[21] H. L. Croad, J. Methven, B. Harvey, S. P. E. Keeley, and A. Volonté, "The role of boundary layer processes in summer-time Arctic cyclones," *Weather and Climate Dynamics*, vol. 4, no. 3, pp. 617–638, 2023.

[22] H. L. Croad, J. Methven, B. Harvey, S. P. E. Keeley, A. Volonté, and K. I. Hodges, "A climatology of summer-time arctic cyclones using a modified phase space," *Geophysical Research Letters*, vol. 50, no. 22, p. e2023GL105993, 2023. e2023GL105993 2023GL105993.

[23] A. F. Vessey, K. I. Hodges, L. C. Shaffrey, and J. J. Day, "The composite development and structure of intense synoptic-scale Arctic cyclones," *Weather and Climate Dynamics*, vol. 3, pp. 1097–1112, Sept. 2022. Publisher: Copernicus GmbH.

[24] M. Yang, Z. Wang, R. M. Rauber, and J. E. Walsh, "Seasonality, latitudinal dependence, and structural evolution of arctic cyclones," *Journal of Climate*, vol. 37, no. 6, pp. 1937 – 1950, 2024.

[25] J.-N. Song, G. Fu, Y. Xu, Z.-Y. Han, Q.-Z. Sun, and H. Wang, "Assessment of the capability of CMIP6 global climate models to simulate Arctic cyclones," *Advances in Climate Change Research*, vol. 12, pp. 660–676, Oct. 2021.

[26] J. J. Day, M. M. Holland, and K. I. Hodges, "Seasonal differences in the response of Arctic cyclones to climate change in CESM1," *Climate Dynamics*, vol. 50, pp. 3885–3903, May 2018.

[27] H. Hersbach, B. Bell, P. Berrisford, S. Hirahara, A. Horányi, J. Muñoz-Sabater, J. Nicolas, C. Peubey, R. Radu, D. Schepers, A. Simmons, C. Soci,

S. Abdalla, X. Abellan, G. Balsamo, P. Bechtold, G. Biavati, J. Bidlot, M. Bonavita, G. De Chiara, P. Dahlgren, D. Dee, M. Diamantakis, R. Dragani, J. Flemming, R. Forbes, M. Fuentes, A. Geer, L. Haimberger, S. Healy, R. J. Hogan, E. Hólm, M. Janisková, S. Keeley, P. Laloyaux, P. Lopez, C. Lupu, G. Radnoti, P. de Rosnay, I. Rozum, F. Vamborg, S. Villaume, and J.-N. Thépaut, "The ERA5 global reanalysis," *Quarterly Journal of the Royal Meteorological Society*, vol. 146, no. 730, pp. 1999–2049, 2020. _eprint: https://onlinelibrary.wiley.com/doi/pdf/10.1002/qj.3803.

[28] G. Danabasoglu, J.-F. Lamarque, J. Bacmeister, D. A. Bailey, A. K. DuVivier, J. Edwards, L. K. Emmons, J. Fasullo, R. Garcia, A. Gettelman, C. Hannay, M. M. Holland, W. G. Large, P. H. Lauritzen, D. M. Lawrence, J. T. M. Lenaerts, K. Lindsay, W. H. Lipscomb, M. J. Mills, R. Neale, K. W. Oleson, B. Otto-Bliesner, A. S. Phillips, W. Sacks, S. Tilmes, L. van Kampenhout, M. Vertenstein, A. Bertini, J. Dennis, C. Deser, C. Fischer, B. Fox-Kemper, J. E. Kay, D. Kinnison, P. J. Kushner, V. E. Larson, M. C. Long, S. Mickelson, J. K. Moore, E. Nienhouse, L. Polvani, P. J. Rasch, and W. G. Strand, "The community earth system model version 2 (cesm2)," *Journal of Advances in Modeling Earth Systems*, vol. 12, no. 2, p. e2019MS001916, 2020. e2019MS001916 2019MS001916.

[29] A. R. Herrington, P. H. Lauritzen, M. Lofverstrom, W. H. Lipscomb, A. Gettelman, and M. A. Taylor, "Impact of grids and dynamical cores in cesm2.2 on the surface mass balance of the greenland ice sheet," *Journal of Advances in Modeling Earth Systems*, vol. 14, no. 11, p. e2022MS003192, 2022. e2022MS003192 2022MS003192.

[30] S.-J. Lin, "A "Vertically Lagrangian" Finite-Volume Dynamical Core for Global Models," *Monthly Weather Review*, vol. 132, pp. 2293–2307, Oct. 2004. Publisher: American Meteorological Society Section: Monthly Weather Review.

[31] E. Blanchard-Wrigglesworth, T. Cox, Z. I. Espinosa, and A. Donohoe, "The largest ever recorded heatwave—characteristics and attribution of the antarctic heatwave of march 2022," *Geophysical Research Letters*, vol. 50, no. 17, p. e2023GL104910, 2023. e2023GL104910 2023GL104910.

[32] A. F. Vessey, K. I. Hodges, L. C. Shaffrey, and J. J. Day, "An inter-comparison of Arctic synoptic scale storms between four global reanalysis datasets," *Climate Dynamics*, vol. 54, pp. 2777–2795, Mar. 2020.

[33] P. A. Bogenschutz and S. K. Krueger, “A simplified pdf parameterization of subgrid-scale clouds and turbulence for cloud-resolving models,” *Journal of Advances in Modeling Earth Systems*, vol. 5, no. 2, pp. 195–211, 2013.

[34] V. E. Larson, “Clubb-silhs: A parameterization of subgrid variability in the atmosphere,” 2022.

[35] A. D. Crawford and M. C. Serreze, “Does the summer arctic frontal zone influence arctic ocean cyclone activity?,” *Journal of Climate*, vol. 29, no. 13, pp. 4977 – 4993, 2016.

[36] K. I. Hodges, “Adaptive Constraints for Feature Tracking,” *Monthly Weather Review*, vol. 127, pp. 1362–1373, June 1999. Publisher: American Meteorological Society Section: Monthly Weather Review.

[37] S. M. Cavallo, “Weather modules,” 2019.

[38] I. Simmonds and E.-P. Lim, “Biases in the calculation of southern hemisphere mean baroclinic eddy growth rate,” *Geophysical Research Letters*, vol. 36, no. 1, 2009.

[39] L. F. Bosart, G. J. Hakim, K. R. Tyle, M. A. Bedrick, W. E. Bracken, M. J. Dickinson, and D. M. Schultz, “Large-scale antecedent conditions associated with the 12–14 march 1993 cyclone (“superstorm ’93”) over eastern north america,” *Monthly Weather Review*, vol. 124, no. 9, pp. 1865 – 1891, 1996.